Biosensors and Bioelectronics 216 (2022) 114641

Contents lists available at ScienceDirect

Biosensors and Bioelectronics

journal homepage: www.elsevier.com/locate/bios

Direct visualization of living bacterial genotypes using CRISPR/Cas12a-circular reporter nanoprobes

Yanan Li [a,1], Yiran Pei [a,1], Di Huang [a], Ru Xu [a], Yonghua Wu [a], Yaqiong Li [a], Ruixue Zhou [a], Yongbin Wei [a], Xiao Tan [c], Hua Gao [b], Jinjin Shi [a], Zhenzhong Zhang [a,**], Kaixiang Zhang [a,***], Jinghong Li [c,*]

[a] School of Pharmaceutical Sciences, Key Laboratory of Targeting Therapy and Diagnosis for Critical Diseases, Collaborative Innovation Center of New Drug Research and Safety Evaluation, State Key Laboratory of Esophageal Cancer Prevention & Treatment, Zhengzhou University, Zhengzhou, 450001, China
[b] Department of Pathogen Biology, School of Basic Medical Sciences, Zhengzhou University, Zhengzhou, 450001, China
[c] Department of Chemistry, Key Laboratory of Bioorganic Phosphorus Chemistry & Chemical Biology, Tsinghua University, Beijing, 100084, China

ARTICLE INFO

Keywords:
Bioassay
Bacterial genotype
CRISPR/Cas12a
Biopolymer materials
In vivo imaging

ABSTRACT

Bacterial genotyping is important for understanding the complex microbiota. Although fluorescence in situ hybridization (FISH) has enabled bacterial community identification with high spatial resolution, its unavoidable cell fixation steps and signal generation by multi-probe stacking greatly limit its application in living bacterial genotyping. Here, we designed polyethyleneimine-encapsulated CRISPR/Cas12a-circular reporter nanoprobes (CasCLR) for rapid and sensitive visualization of gene information in living bacteria. We found that, nanoprobe-based sequential delivery of Cas12a/crRNA and circular reporter into bacteria allowed single genomic loci to initiate trans-cleavage activity of Cas12a, thereby cleaving CLR to generate amplified fluorescent signals for imaging of target gene. Using CasCLR, we can sensitively analyze the percentage of target bacteria in co-culture experiments and directly detect pathogenic bacteria in uncultured mouse gut microbe. In addition, CasCLR has the ability to sensitively analyze specific genotype of microbial communities *in vivo*. This nanobiotechnology-based bacterial gene analysis is expected to advance understanding of *in vivo* bacterial cytogenetic information.

1. Introduction

Classification of bacteria is the first step for bacterial community research and treatment of clinical infection (Kwon et al., 2019; Peukert et al., 2022; Xing et al., 2021). Conventional bacteria classification steps are mainly based on phenotypic features, such as cellular composition, cellular metabolism and cellular structure (Lim et al., 2019; Parks et al., 2018), which have been widely used but lacks genetic information in taxonomic classification. With the development of polymerase chain reaction (PCR) (Shang et al., 2005), fluorescence in situ hybridization (FISH) (Mark Welch et al., 2017) and next generation sequencing (NGS) (Elmentaite et al., 2021; Gosiewski et al., 2017), genetic analysis methods are regarded as more powerful techniques for bacterial identification.

Among them, FISH is a molecular cytogenetic technique that utilizes fluorescent DNA probes with high sequence complementarity to target bacterial 16S rRNA for in situ visualization and identification of microorganisms (Mark Welch et al., 2017; Ranasinghe et al., 2018; Valm et al., 2011; Wagner et al., 2003). The newly developed FISH technology, such as CLASI-FISH (combinatorial labeling and spectral imaging) strategy (Valm et al., 2011) and high-phylogenetic-resolution FISH (HiPR-FISH) technique (Shi et al., 2020), can provide rich information on the spatial distribution of gut microbe, which is helpful for understanding the structure and organization of microbial communities at the micron level. However, limited by the high degree of sequence conservation of subunits of 16S rRNAs, FISH is generally not suitable for distinguishing microbe below the species level (Lee et al., 2022). Furthermore, the necessary cell fixation steps, complex probe designs,

* Corresponding author.
** Corresponding author.
*** Corresponding author.
E-mail addresses: zhangzhenzhong@zzu.edu.cn (Z. Zhang), zhangkx@zzu.edu.cn (K. Zhang), jhli@mail.tsinghua.edu.cn (J. Li).
[1] These authors contributed equally: Yanan Li, Yiran Pei.

https://doi.org/10.1016/j.bios.2022.114641
Received 5 July 2022; Received in revised form 6 August 2022; Accepted 14 August 2022
Available online 19 August 2022
0956-5663/© 2022 Published by Elsevier B.V.

long time-cost and labor-intensive experimental procedures greatly hinder its applications (Lin et al., 2021a). To date, sensitive and rapid imaging of living bacterial genotypes in different environments without fixation is still a challenge.

The clustered regularly interspaced short palindromic repeats (CRISPR) system, which consists of a CRISPR-associated (Cas) nuclease and a guide RNA (gRNA), is a powerful gene editing system developed in recent years (Dai et al., 2020). Beyond its remarkable genome editing ability, recent advances toward CRISPR system have provided a new molecular recognition tool for displaying genetic information in living cells with high spatiotemporal resolution (Feng et al., 2021; Knight SC et al., 2017; Teng et al., 2022; Zhang et al., 2022). Of these, the CRISPR/Cas12a effector protein, which is an RNA-guided nuclease that binds and cleaves target DNA to activate trans-cleavage activity for indiscriminately reducing nearby single-stranded DNA (ssDNA) molecules, deserves attention (Chen et al., 2018; Kleinstiver et al., 2019). This collateral ssDNA cleavage capability led to the development of Cas12a system as a highly efficient nucleic acid diagnostic tool, such as SHERLOCK (Gootenberg et al., 2018) and DETECTR (Chen et al., 2018), for sensitive detection of multiple clinical nucleic acid biomarkers (Feng et al., 2021). Moreover, such attractive features have been employed to achieve live-cell biosensing applications (Chen et al., 2022; Huang et al., 2021; Pan et al., 2022; Wang et al., 2022). Unlike FISH which needs probes stacking to generate fluorescent signal, Cas12a enables single crRNA-mediated generation of amplified fluorescent signals by targeting a single genetic locus. This property enables microbe distinguish below the species level with subtle 16S rRNAs variation. Nonetheless, Cas12a-based probes have not been applied for living bacterial genotyping, due to the challenges of efficient living bacteria delivery of Cas12a probes and fluorescent reporter groups.

In this work, we developed CRISPR/Cas12a-circular reporter nanoprobes (CasCLR) for visualizing genotypes of living bacteria, which uses polymer biomaterials-polyethyleneimine (PEI) as the transfection vector for CRISPR/Cas12a effectors and circular reporter (CLR) designed to avoid non-specific signals (Fig. 1). As a non-viral gene carrier with a high density of positive charges, PEI can be stably combined with Cas12a/crRNA complex and CLR to form uniform spherical complex to achieve safe and efficient bacterial transformation. On the other hand, the design of CLR greatly improved the stability of fluorescent reporters in living bacteria to ensure the accuracy of CasCLR detection of target gene fragment.

We found that the high fidelity of base pairing between crRNA and target dsDNA allow CasCLR to recognize sophisticated target genotypes in a variety of living bacteria. With the robust fluorescent signal generated by CasCLR targeting single copy genomic loci, we can differentiate bacterial subtypes and sensitively analyze the percentage of target bacteria in complex samples. Furthermore, the practical ability of CasCLR to image target bacterial genotypes in uncultured complex bacterial communities (the mouse gut microbiota) was demonstrated. In addition, CasCLR enables specifically analysis of bacterial genotypes in superficial tissues. With excellent reliability, sensitivity, and ease of implementation, this method offers great potential for real-time analysis of *in vivo* bacterial community heterogeneity and distributional composition.

2. Materials and methods

For experimental details, please refer to the supplementary information.

3. Results and discussion

3.1. Design and characterization of CasCLR

To deliver Cas12a and fluorescent reporter probes into living bacteria, the first challenge to overcome is the complex cell wall located on the outermost layer of bacterial cells, wraps around the cell membrane (Liu et al., 2021; Pasquina-Lemonche et al., 2020). Cationic polymers is one of the most widely used carrier materials for gene delivery (e.g. siRNA, plasmid DNA) and is available in branched or linear types of various molecular weights (Chen et al., 2022). We firstly investigated the oligonucleotide transfection efficiency of different cationic polymers, including polyamidoamine (PAMAM)(Wu et al., 2021), polylysines (PLL) (Laurino et al., 2011), and branched polyetherimides (PEI) (Kang et al., 2017) of different molecular weights, respectively (Fig. S1A). Particle size and Zeta potential of different transfection agents indicated that PEI 1000 and PEI 25000 encapsulate oligonucleotides to form smaller nanoparticles and carry a positive charge that facilitates bacterial uptake (Fig. S1B). Then flow cytometry results demonstrate that PEI with a molecular weight of 1000 can efficiently deliver DNA probes into bacteria (Fig. S1C). These results encouraged us to use PEI 1000 to construct nanoprobes for transient transfection of oligonucleotides into living bacteria (Fig. 2A).

Although PEI has been employed for the delivery of various genetic medicines, it still has certain cytotoxicity issue (Haldar et al., 2006). To this end, the ratio of Cas12a protein in different PEIs were investigated (Fig. S2). The confocal imaging results of living bacteria showed that the fluorescence intensity of bacteria was positively correlated with the mass of PEI (Fig. S2A). However, the significant change of bacterial morphology illustrates the potential cytotoxicity of the PEI. Then, mini broth dilution susceptibility test was used to investigate the cytotoxicity of Cas12a protein transfected with different mass of PEI (Fig. S2B).

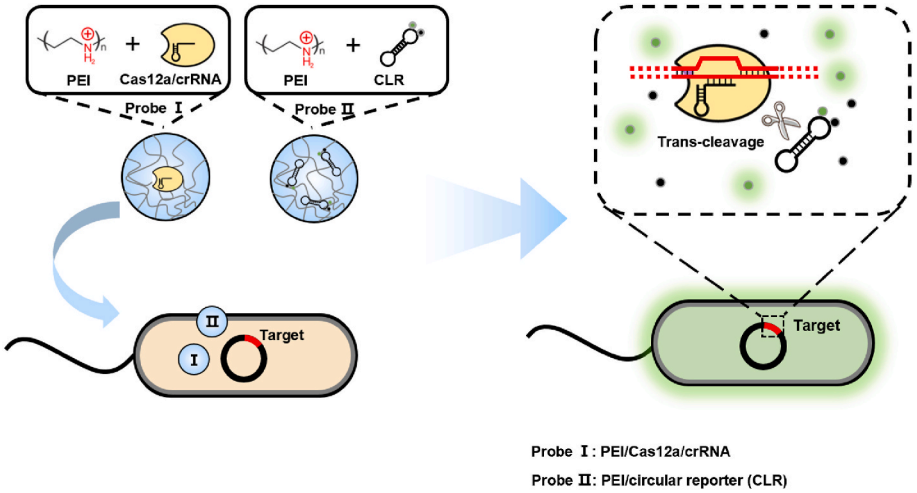


Fig. 1. Design of CRISPR/Cas12a-circular reporter nanoprobes (CasCLR) for visualizing living bacteria genotype. Firstly, polyethyleneimine (PEI, MW = 1000) encapsulated Cas12a/crRNA complex is delivered into the bacteria as probe I, which identifies target gene and activates the trans-cleavage activity of Cas12a. Secondly, PEI encapsulated circular reporter (CLR) is delivered into the bacteria as probe II, which is cleaved by Cas12a, lighting up to show the genotype of target bacteria.

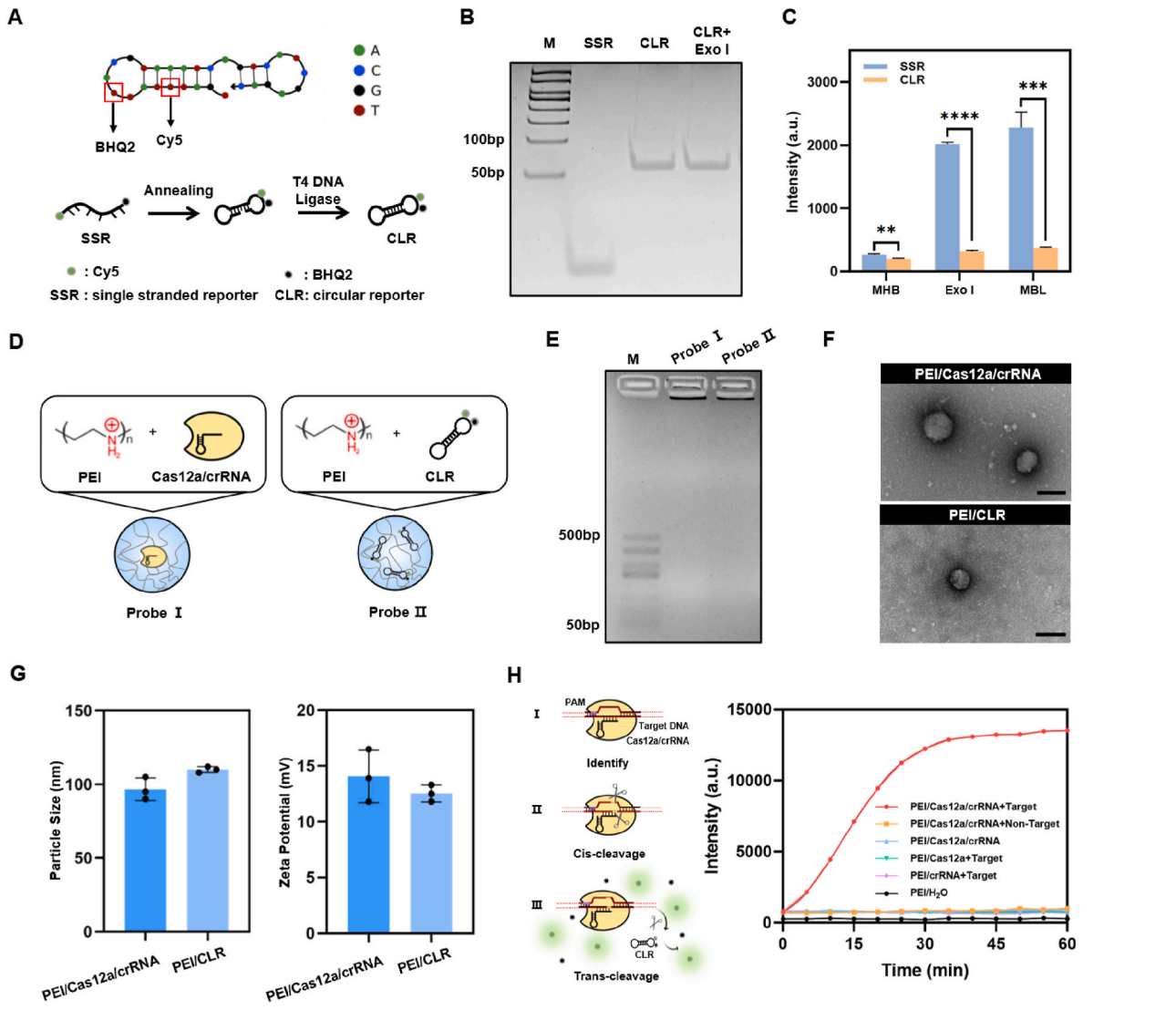


Fig. 2. Design and characterization of CasCLR. (A) Design of CLR. Detailed sequence information is provided in Table S1. (B) Polyacrylamide gel electrophoresis (PAGE) analysis of the assembly process of CLR. (C) Stability analysis of SSR and CLR after incubation with Mueller-Hinton Broth (MHB) medium, 0.25 U/μL Exo I and mechanical bacterial lysate (MBL) for 1 h. (D) Design of two nanoprobes for bacteria targeting delivery. Probe I: PEI encapsulated Cas12a/crRNA complex; Probe II: PEI encapsulated CLR. (E) Agarose gel electrophoresis analysis of PEI encapsulated Cas12a/crRNA (lane I) and CLR (lane II) forming nanoparticles, respectively. (F) TEM characterization of PEI/Cas12a/crRNA and PEI/CLR probes. Scale bar, 100 nm. (G) Particle size (left) and zeta potential (right) of PEI/Cas12a/crRNA and PEI/CLR probes. (H) *In vitro* real-time fluorescence assay of target gene activated PEI/Cas12a/crRNA trans-cleavage.

These results indicated that the optimal ratio of PEI/Cas12a/crRNA nanoprobes was 10.

Since bacteria contain and keep secreting many kinds of nucleases, the classical CRISPR/Cas12a fluorescent reporter, which is a 5 nt short ssDNA (FAM-TTATT-BHQ1), is not suitable for sensing gene information in living bacteria. In recent years, the circularization strategy, which utilizes DNA ligase to ligate single-stranded oligonucleotides into circular structures, has been used to obtain oligonucleotide drugs with high *in vivo* stability (Zhang et al., 2020). Therefore, we hypothesized that a circular reporter (CLR) may display enhanced stability in living bacterial environment.

The design of CLR is shown in Fig. 2A. Specifically, the commonly used fluorescent reporter group of Cas12a, Cy5-TTATT-BHQ2, was extended by 4 nt and 21 nt at the 5 and 3 ends, respectively, which named ssDNA reporter (SSR). After annealing and cooling to room temperature, the dumbbell-shaped structures with 1 nick were sealed using T4 DNA ligase. The TTATT motif preferentially cleaved by Cas12a is at end of the CLR dumbbell-shaped structure and remains single-stranded. Synthesized CLR was initially characterized by polyacrylamide gel electrophoresis (Fig. 2B). The band that moved up obviously did not change significantly after the exonuclease treatment, which proved the successful preparation of the closed-loop structure. By semi quantifying the intensity of the main band and other residual bands of the gel, the yield of CLR was estimated to be ~ 84%.

Subsequently, we investigated the stability of CLRs under different physiological conditions using gel electrophoresis and *in vitro* fluorescence assay. The CLR structure is resistant to cleavage by exonuclease I (Fig. S3), and its stable structure prevents nonspecific fluorescent signals in bacterial extracts (Fig. 2C), setting the stage for accurate responses of Cas12a trans-cleavage activity in living bacteria. The responsiveness of CLRs to target-initiated Cas12a trans-cleavage activity was subsequently assessed (Figs. S4A–C). The significantly enhanced fluorescence signal of CLR in the presence of target suggests that the circular structure does not affect its ability to serve as a substrate for Cas12a nuclease.

To prepare PEI/CLR (PEI encapsulated circular reporter), we compared the bacterial transformation efficiency of PEI/DNA complexes with different PEI/DNA ratios (also known as nitrogen-to-phosphorus, N/P ratios) (Fig. S5). Agarose gel electrophoresis, particle size and

Zeta potential results showed that when N/P = 8, PEI and DNA formed nanoparticles, maintaining a small particle size and carrying a positive charge (Figs. S5A–B). In addition, flow cytometry proved that when N/P = 8, PEI/DNA nanoparticles can efficiently enter bacteria (Fig. S5C). Therefore, we choose an N/P ratio of 8 to construct PEI/CLR.

According to the above optimized conditions, we synthesized two kinds of nanoprobes, PEI/Cas12a/crRNA and PEI/CLR, respectively. Agarose gel electrophoresis analysis showed that both the Cas12a/crRNA complex and CLR formed nanoparticles with PEI (Fig. 2E). The results of transmission electron microscopy (TEM) showed that the two probes of CasCLR were both with regular spherical shape (Fig. 2F), the diameter of PEI/Cas12a/crRNA and PEI/CLR were 96.67 ± 6.24 nm and 110 ± 1.63 nm, respectively (Fig. 2G). Both probes for CasCLR are positively charged (Fig. 2G), favorable for binding to living bacteria and transient transfection. To verify that the PEI-encapsulated Cas12a/crRNA complex still possesses target-initiated trans-cleavage activity, a fluorescent reporter cleavage study was performed. In the absence of DNA activator, minimal fluorescence signal was observed. When CLR was incubated with PEI/Cas12a/crRNA and DNA activator, a considerable fluorescence signal was shown (Fig. 2H), indicating that the Cas12a/crRNA complex in PEI maintained efficient trans-cleavage ability after recognizing target DNA. Therefore, CasCLR is expected to enter bacteria and report target DNA, enabling the visualization of different bacterial genotypes.

3.2. CasCLR for imaging target gene loci in living bacteria

To test the ability of CasCLR to detect specific genotype in living bacteria, we used *NDM-1* gene as a proof-of-concept model. NDM-EC1322 bacteria, an *E. coli* isolate produced by clinical NDM-1 (a most common NDM isoform) (Dong et al., 2022), were first examined for uptake of PEI/CLR and PEI/Cas12a/crRNA using flow cytometry (Fig. S6). The selected NDM-EC1322 antibiotic-resistant bacteria was subsequently sequenced to confirm it contained the target *NDM-1* gene loci (Fig. S7). According to the sequencing results, we designed a single crRNA for a 20 bp site in the *NDM-1* gene to construct $CasCLR_{NDM\text{-}1}$.

The effect of co-delivery and sequential delivery of CasCLR to living bacteria were firstly tested (Fig. S8). When Cas12a/crRNA and CLR were co-delivered with a small amount of PEI, no obvious fluorescent signal was found in the bacteria. Although increasing the amount of PEI can significantly improve the delivery efficiency to generate a fluorescent signal comparable to that of sequential delivery, the confocal images showed significant changes in bacterial morphology, demonstrating the high toxicity of this method to bacteria. This result drive us to explore

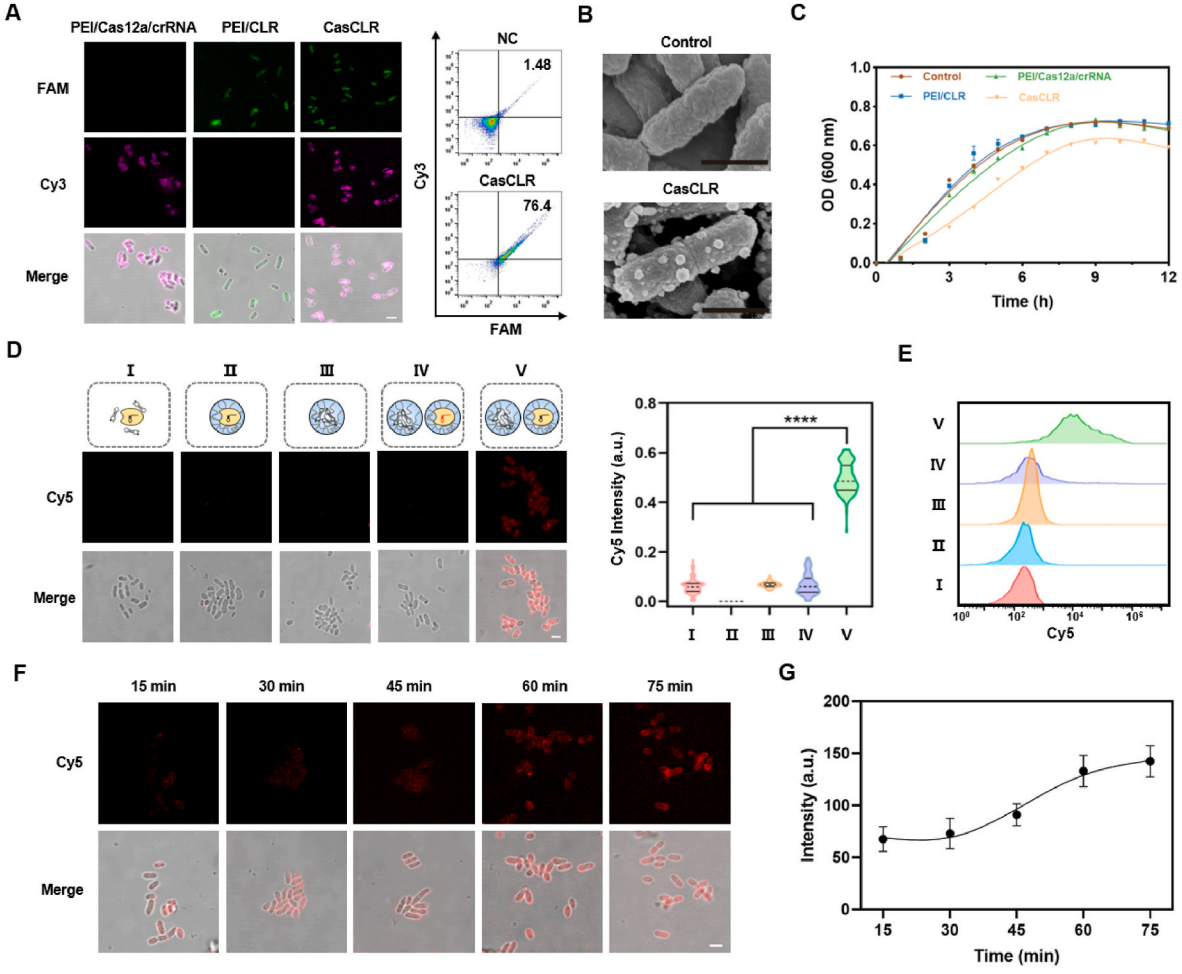


Fig. 3. CasCLR for imaging *NDM-1* gene in living NDM-EC1322 bacteria. (A) Analysis of NDM-EC1322 bacteria uptake PEI/Cas12a/crRNA probe, PEI/CLR probe, and both of them. Scale bar, 1 μm. Confocal imaging is on left panel and the flow cytometry analysis is on the right. (B) Bio-SEM characterization of NDM-EC1322 bacteria incubated with PEI/Cas12a/crRNA (100 nM) for 30 min and PEI/CLR (2.5 μM) for 1 h. Scale bar, 1 μm. (C) Analysis of the toxicity of different probes to NDM-EC1322 bacteria, n = 3 independent experiments. (D) Confocal imaging of NDM-EC1322 bacteria treated with different probes. I: Cas12a/crRNA; II: PEI/Cas12a/crRNA; III: PEI/CLR; Ⅳ: $CasCLR_{NT}$; V: $CasCLR_{NDM\text{-}1}$. Scale bar, 1 μm. Semi-quantitative analysis of the fluorescence intensity in each bacterium is shown on the right. n = 50. (E) Flow cytometry analysis of each group corresponding to panel D. (F) Time-lapse confocal imaging of NDM-EC1322 bacteria incubated with CasCLR for different time interval. Scale bar, 1 μm. (G) Mean fluorescence intensity of bacteria in panel F over time. n = 50.

sequential delivery of CasCLR for imaging of living bacterial genotypes.

When PEI/Cas12a/crRNA and PEI/CLR were delivered sequentially, the green fluorescence of PEI/CLR and purple fluorescence of PEI/Cas12a/crRNA had good co-localization, with a Pearson's correlation coefficient (PCC) of 0.40 (Fig. 3A). Although the separate delivery of the two probes caused non-uniformity in bacterial uptake, i.e., inconsistent green and purple fluorescence intensities for some bacteria, flow cytometry showed that after the sequential delivery of PEI/Cas12a/crRNA and PEI/CLR, up to 76.4% of bacteria were double positive for FAM and Cy3 (Fig. 3A). The result of scanning electron microscope (SEM) indicated that the morphology and integrity of NDM-EC1322 bacteria did not change significantly before and after the uptake of CasCLR (Fig. 3B).

After checking the toxicity of CasCLR to bacterial cells (Fig. 3C), we tried to image genotype in living NDM-EC1322 bacteria with the developed nanoprobes. As shown in Fig. 3D, after treated with $CasCLR_{NDM-1}$, strong red fluorescence signals were observed in 78% living NDM-EC1322 bacteria, while no obvious signal was observed in other treated NDM-EC1322 bacteria. Semi-quantitative analysis of fluorescence intensity (Fig. 3D) and flow cytometry analysis (Fig. 3E) further confirmed these results, demonstrating successful detection of specific genomic region in living bacteria using CasCLR. As shown in Fig. S9, fluorescence signals are only observed in NDM-EC1322 bacteria when mammalian cells spiked with NDM-EC1322 bacteria are treated with $CasCLR_{NDM-1}$ for 1 h, confirming the specificity of CasCLR for bacteria.

Using a cyclization strategy, CLR has shown superior stability and Cas12a nuclease responsiveness *in vitro*, and we subsequently examined its application in living bacteria imaging. As shown in Fig. S10A, when the fluorescent reporter group was delivered into the living bacteria, the nuclease resistance of CLR provides extremely low non-specific background signals compared to SSR. In the presence of the Cas12a/crRNA complex, the target-initiated trans-cleavage activity can rapidly cleave CLR, showing strong signal amplification ability (Figs. S10B–C). The signal-to-background ratio (S/B) of CasCLR (~33.85) was more than ~14.5 fold higher than that of CasSSR (~2.34). These results indicated that CasCLR achieve high signal-to-noise ratio for more accurate sensing of living bacterial gene information.

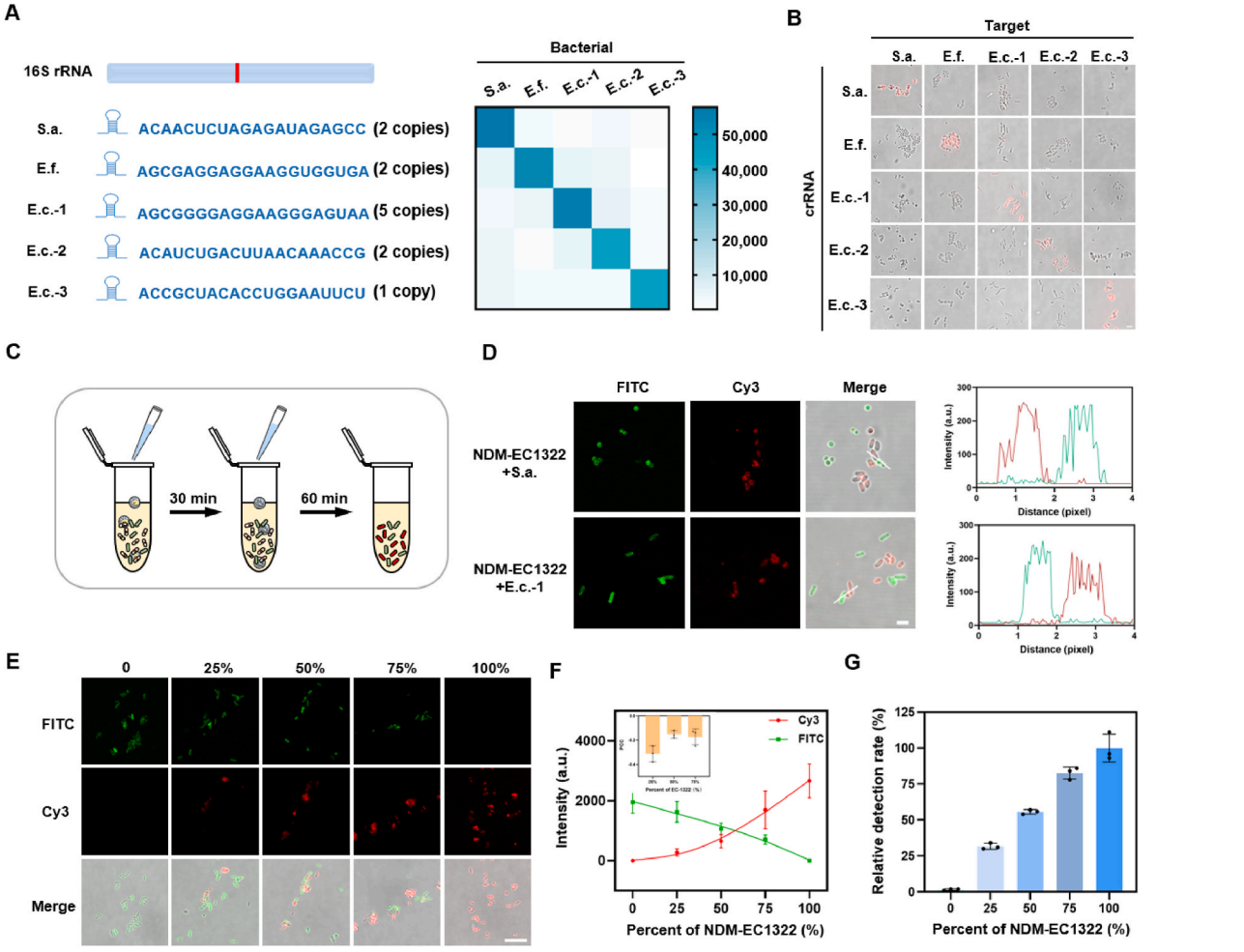


Fig. 4. Quantitative analysis of NDM-EC1322 bacteria content in a co-culture system. (A) crRNA sequence information (left) for bacteria identification based on 16S rRNA target region. S.a.: *Staphylococcus aureus* (ATCC 29213); E.f.: *Enterococcus faecalis* (ATCC 29212); E.c.-1: *Escherichia coli* (ATCC 25922); E.c.-2: *Escherichia coli* (BL 21); E.c.-3: *Escherichia coli* Nissle 1917. Heat map (right) analysis of *in vitro* fluorescence assay for orthologous identification of bacteria based on statistics from 3 independent experiments. (B) Confocal imaging analysis of orthologous identification of bacteria using CasCLR. Scale bars, 1 μm. (C) Schematic diagram of CasCLR's for selective imaging of target bacteria in a co-culture system. (D) Confocal imaging of NDM-EC1322 bacteria (Red) with S.a. or E.c.-1 (Green). S.a.: *Staphylococcus aureus* (ATCC 29213); E.c.-1: *Escherichia coli* (ATCC 25922). Scale bar, 1 μm. S.a. or E.c.-1 were cultured overnight in MHB medium supplemented with FITC-d-Lys (100 μM) for pre-label with FITC. (E) Imaging of different percentage of NDM-EC1322 bacteria (Red) and E.c.-1 (Green) in a bacteria co-culture system, E.c.-1 bacteria were pre-labeled with FITC-d-Lys. Scale bar, 10 μm. (F) Semi-quantitatively analyze the changes of different percentage of two bacteria of fluorescence intensity to panel E by Fiji. Inset shows the corresponding PCC analyze of green and red fluorescence in panel E by Fiji. (G) Flow cytometry analysis relative detection rate of each group corresponding to panel E. n = 3, data show mean ± SD.

Subsequently, time-lapse confocal imaging of NDM-EC1322 bacteria incubated with CasCLR (Fig. 3F) was performed to test the optimal timing of CasCLR for gene sensing in live bacteria. After 30 min of incubation, red fluorescence generated by CasCLR in individual NDM-EC1322 bacteria raised with time and reaching a plateau at around 60 min (Fig. 3G). Besides, it was found that, NDM-EC1322 maintained its moving ability after incubation with CasCLR, demonstrating the living bacteria imaging application. Considering the tradeoff between time and detection efficiency, we chose incubation time of 60 min to achieve bacterial genotype imaging.

3.3. Bacterial genotyping and quantitative monitoring of NDM-EC1322 bacteria fluctuations in co-culture models

Although FISH has been used for bacterial identification for decades, continued advances in microbial genomics research have created new challenges for finer bacterial genotyping due to its insensitivity to highly homologous shorter (<20 bp) genetic information (A M Pirttilä 2000; Greuter et al., 2016). To further evaluate the genotyping ability of CasCLR as assured by the macromolecular recognition ability of Cas12a, we selected 2 Gram-positive bacterial and 3 Gram-negative bacterial to test the specificity of CasCLR, and the result is shown as a heat map in Fig. 4A. CasCLR detects all living bacteria using crRNA targeted a species-specific low copy site in the 16S rRNA gene. Each CasCLR selectively responded to genome from its target bacterial with a low cross-response. Furthermore, confocal imaging assays were employed to investigate the orthogonal specificity of CasCLR in genotyping of living bacteria. As shown in Fig. 4B, the red fluorescent signal produced by CasCLR was only found inside target bacteria rather than other different types of bacteria. These results indicated that CasCLR can analyze the genotypes of both Gram-positive bacteria and Gram-negative bacteria, and has the ability to sensitively distinguish different subtypes of the same kind bacteria.

Given that CasCLR shows great excellence in bacterial homology identification, we first validated the utility of CasCLR in analyzing the genotypes of target bacteria in different bacterial co-culture models. A 1:1 mixture of NDM-EC1322 and FITC-labeled *Escherichia coli* (ATCC 25922, E.c.-1) or *Staphylococcus aureus* (ATCC 29213, S.a.) was sequentially incubated with the two probes of CasCLR for 1.5 h and analysed by confocal imaging (Fig. 4C). When incubated with FITC-labeled Gram-positive (S.a. ATCC 29213) or Gram-negative bacteria (E.c.-1, ATCC 25922), only NDM-EC1322 bacteria showed red fluorescent signals generated by CasCLR (Fig. 4D). The spatial co-localization of Cy3 fluorescence signal and FITC fluorescence signal further states CasCLR can detect living bacteria containing target gene in co-culture model.

Subsequently, we attempted to evaluate the detection sensitivity of CasCLR. After treated co-cultured bacteria with different ratio of NDM-EC1322: FITC-labeled *E. coli* ATCC 25922 (0, 25, 50, 75, 100%) using CasCLR (Fig. 4E–G). Confocal imaging of living bacteria showed red fluorescence signal produced by CasCLR increased with the increase of NDM-EC1322 bacteria ratio, and did not co-localize with the decreasing green fluorescence signal (Fig. 4E and F). The results of flow cytometry further showed that the proportion of Cy3 signal in the co-culture model increased with the proportion of NDM-EC1322 bacteria (Fig. S11). After normalizing all groups, the proportion of Cy3-positive bacteria closely matched the proportion of NDM-EC1322 bacteria (Fig. 4G). These results demonstrate that CasCLR can rapidly detect living bacteria containing target genotypes in bacteria co-culture environments, laying the foundation for bacterial community research and clinical infection analysis.

3.4. CasCLR for detecting NDM-EC1322 bacteria in uncultured mouse gut microbiota

Imaging of living bacterial genotype has broad applications in understanding the complex microbiota that exist on or within our bodies. Yet, due to the lack of suitable tools for distinguishing specific bacteria species *in vivo*, it remains a significant challenge (Daims and Wagner, 2007; Earle et al., 2015; Shi et al., 2020). To this end, we attempted to employ CasCLR to detect living bacteria of a specific genotype in a heterogeneous bacterial community. Using NDM-EC1322 bacteria as a model with antibiotic-resistant gene, we investigated its distribution in the complex environment of gut microbe (Fig. 5A). Specifically, we administered FITC-labeled NDM-EC1322 bacteria to C57 mice by gavage. After 12 h, the microbe of their ileum, cecum and colon were extracted respectively. PCR and sanger sequencing analysis of the *NDM-1* gene confirmed colonization of the gut by NDM-EC1322 bacteria (Fig. S12). After incubating with CasCLR, bacteria containing FITC and Cy3 fluorescence signals were detected using laser confocal microscope and flow cytometry, respectively. An obvious red fluorescence signal appeared in the gut microbiota, co-localized well with the green fluorescence of FITC, and the red fluorescence in the colon was significantly weaker than that in the ileum and cecum (Fig. 5B, Fig. S13). Notably, the morphology of identified NDM-EC1322 bacteria in mouse gut was significantly different from *in vitro* study, possibly due to the differences in culture environment, such as intestinal pH, oxygen partial pressure levels, and mucopolysaccharide levels (Lin et al., 2021b).

Flow cytometry showed around 7.42% and 7.39% of FITC and Cy3 double-positive bacteria detected in the ileum and cecum, only 5.02% in the colon (Fig. 5C), which show similar tendency as the confocal imaging results. In addition, some bacteria with only green or red fluorescence were observed. This may because the heterogeneity of sequential delivery (Fig. 3A), inevitable self-fluorescence of gut flora, loss of fluorescent label, or the transmission of genetic information between bacteria (Carattoli, 2009). All these possibilities further illustrate the challenge of living bacteria genotyping in complex physiological environment.

3.5. CasCLR for imaging specific bacteria in superficial tissues

In vivo identification of bacteria has been a long-sought goal. Although nanoparticles that rely on bacterial-specific uptake are able to detect bacterial distribution in mouse models (Tang et al., 2019), they cannot provide further detailed information such as bacterial types. One major advantage of CasCLR is its low-copy-specific locus-responsive fluorescence signal, which has the potential for *in vivo* imaging of bacteria containing specific loci. To demonstrate that the CasCLR have the potential to specifically genotype bacteria *in vivo*, two bacteria-infected mice models are constructed (Fig. S14). First, we examined the superior stability of CLR in *in vivo* imaging (Fig. S15A). As shown in Fig. S15, PEI/SSR produced significant autofluorescence in bacterially infected epidermal tissue, whereas no fluorescent signal was observed at the PEI/CLR -injected infection site, demonstrating that the cyclization-designed CLR has significantly improved *in vivo* stability.

Then, mouse models with NDM-EC1322 bacterial infection sites on the left and right forelimbs were treated with in situ injection of PEI/Cas12a, PEI/CLR, $CasCLR_{NT}$ and $CasCLR_{NDM-1}$(Fig. 6A). As shown in Fig. 6B, compared with other different treatment groups, the left infection site of $CasCLR_{NDM-1}$ group showed obvious fluorescent signal. *Ex vivo* fluorescence imaging of the infection site also showed similar results (Fig. 6C), indicating that only $CasCLR_{NDM-1}$ specifically recognize the *NDM-1* gene to obtain a significant fluorescence signal at the infection site. In addition, there were obvious fluorescent signals in the abdomen of mice in each group, which mainly existed in the gastrointestinal tract (Fig. S16), possibly from autofluorescence from feed and feces (Kwon and Sevick-Muraca, 2017).

To test the specificity of CasCLR for *in vivo* imaging of bacterial genotypes, a mouse model of bilateral xenogeneic bacterial infection was constructed (Fig. 6D–F). After $CasCLR_{NDM-1}$ treatment, only the NDM-EC1322 infection site had obvious fluorescent signal (Fig. 6D). A distinct fluorescent signal was observed only at the infection site of

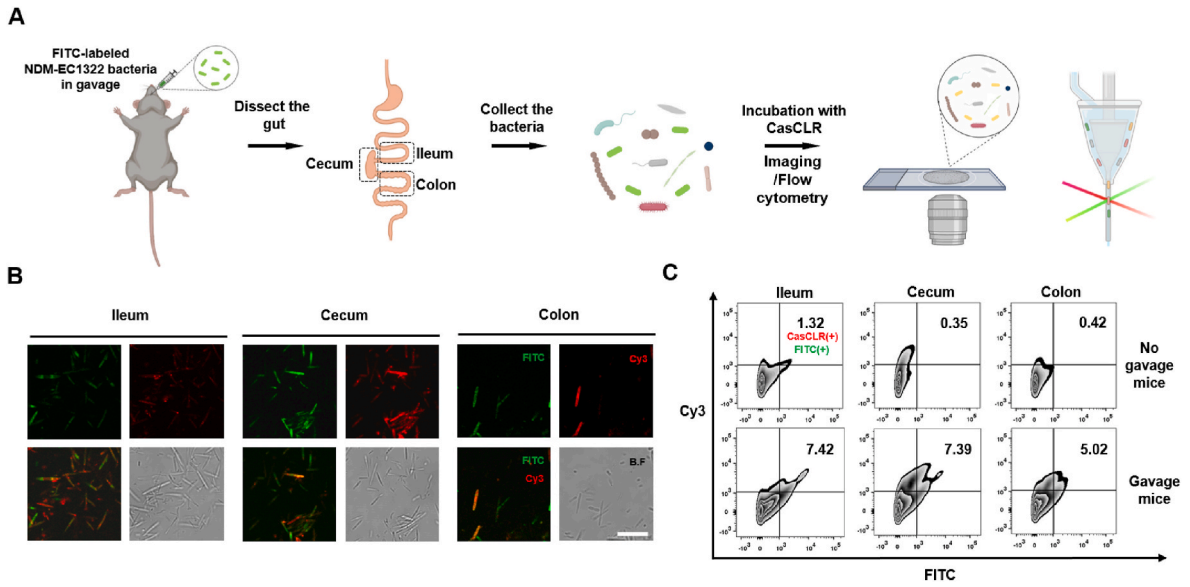


Fig. 5. Detection of gavaged NDM-EC1322 bacteria in the mouse gut using CasCLR. (A) Schematic illustration of CasCLR for the detection of NDM-EC1322 bacteria in the mouse gut. The gavaged NDM-EC1322 bacteria were pre-labeled with FITC-d-Lys. (B) Imaging of NDM-EC1322 bacteria labeled with FITC (green) in the gut microbiota using CasCLR (red). NDM-EC1322 bacteria were imaged in the ileum, cecum and colon, respectively. Scale bar, 10 μm. Representative images from at least three independent experiments are shown. BF, bright field. (C) Flow cytometry analysis of each group corresponding to panel B.

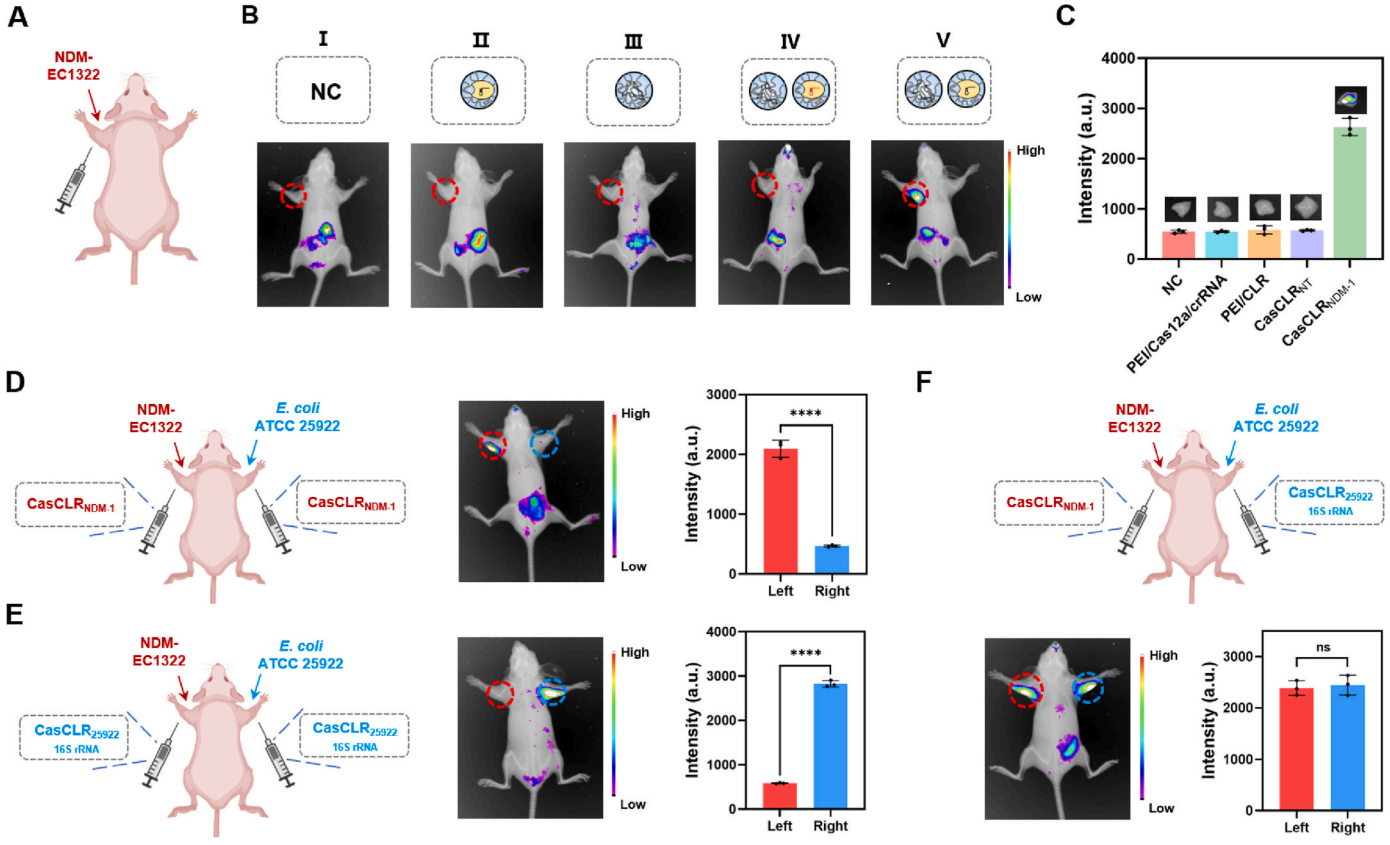


Fig. 6. ***In vivo*** **imaging of bacteria with specific genotype in infected mouse model using CasCLR**. (A) Schematic of in situ injection of $CasCLR_{NT}$ or $CasCLR_{NDM\text{-}1}$ into a mouse model bearing with NDM-EC1322 bacterial infection sites on the left forelimbs to detect *NDM-1* gene *in vivo*. (B) *In vivo* imaging of NDM-EC1322 bacterial infected mice after injection of $CasCLR_{NT}$ or $CasCLR_{NDM\text{-}1}$. The experiment was independently repeated three times with similar results. (C) Evaluation of the fluorescence intensity of dissected mouse infected tissue. n = 3, data show mean ± SD. (D–F) Schematic of in situ injection of $CasCLR_{NDM\text{-}1}$ (D) or $CasCLR_{25922\ 16S\ rRNA}$ (E) into a dual-infect mouse model (bearing an NDM-EC1322 bacterial infected site (NDM-EC1322) on the left (Red circle) and an *E. coli* ATCC 25922 bacterial infected site (*E. coli* ATCC 25922) on the right (Blue circle)) to detect specific gene loci *in vivo*.

E. coli ATCC 25922 bacteria after $CasCLR_{25922\ 16s\ RNA}$ treatment (Fig. 6E). When the corresponding CasCLR was injected in situ, a fluorescent signal was observed at both sites of infection (Fig. 6F). *In vitro* fluorescence imaging of infection sites and major organs further demonstrated the ability of CasCLR to accurately image bacterial communities carrying target genes *in vivo* (Fig. S17). These findings indicated that CasCLR is capable of specifically discriminating bacterial genotypes *in vivo*.

4. Conclusion

Bacterial genotyping has broad applications in understanding the complex microbial lineages. Here, we report polyethyleneimine-encapsulated CRISPR/Cas12a-circular reporter nanoprobes for visualizing genomic information in living bacterial, which demonstrates robust genotyping capabilities for different types of living bacteria *in vivo* (Table S3). PEI can encapsulate CRISPR/Cas12a and CLR respectively to form spherical nanoparticles, efficiently delivered CasCLR probes to the interior of living bacteria sequentially, in which Cas12a as both sensing and reporting system to detection low-copy gene loci; CLR as signal amplification system to increase the signal-to-noise ratio by 14.5-fold.

For different bacteria (Gram-positive and Gram-negative) of different genotypes, CasCLR showed strong orthogonal identification of bacterial homology. It can sensitively detect trace amounts of target bacteria in co-culture environments with single bacteria resolution. Moreover, CasCLR can be applied not only to the imaging analysis of cultured bacteria, but to the analysis of target bacteria colonizing in the mouse gut without culture. In addition, CasCLR exhibits excellent capability for *in vivo* bacterial genotyping. The uneven distribution of probes caused by step-by-step delivery limits imaging efficiency, which is expected to be solved by integrating Cas12a/crRNA and CLR to form an integrated nanoprobe. Nanotechnology-based CasCLR probes have unique and powerful properties that enable previously difficult studies, such as real-time *in vivo* imaging of bacterial community composition and distribution with high selectivity and sensitivity.

CRediT authorship contribution statement

Yanan Li: Conceived the project and designed the experiments, Methodology, Data curation, and, Writing-original draft. **Yiran Pei:** Conceived the project and designed the experiments, Methodology, Data curation, and, Writing-original draft. **Di Huang:** Writing – review & editing. **Ru Xu:** Methodology, Data curation. **Yonghua Wu:** Methodology, Data curation. **Yaqiong Li**: Analysed the results. **Ruixue Zhou:** Analysed the results. **Yongbin Wei:** Analysed the results. **Xiao Tan:** Methodology, Supervision. **Hua Gao:** Methodology, Supervision. **Jinjin Shi:** Supervised the entire project. **Zhenzhong Zhang:** Supervised the entire project. **Kaixiang Zhang:** Conceptualization, Methodology, Project administration, Supervision, Funding acquisition, Writing–review & editing. **Jinghong Li:** Project administration, Supervision, Writing–review & editing.

Declaration of competing interest

The authors declare that they have no known competing financial interests or personal relationships that could have appeared to influence the work reported in this paper.

Data availability

Data will be made available on request.

Acknowledgements

This work was supported by grants from the National Natural Science Foundation of China (Nos. 21904119, U2004197, 22122409), Program for Science & Technology Innovation Talents in Universities of Henan Province (No. 21HASTIT043), Key Scientific Research Projects (Science and Technology Department of Henan Province, no. 222102310011). All the animal experiments were performed in accord with the guidelines of the Regional Ethics Committee for Animal Experiments and Zhengzhou University Institutional Animal Care and Use Committee. The authors thank Modern Analysis and Computing Center of Zhengzhou University for technical assistance.

Appendix A. Supplementary data

Supplementary data to this article can be found online at https://doi.org/10.1016/j.bios.2022.114641.

References

Carattoli, A., 2009. Antimicrob. Agents Chemother. 53 (6), 2227–2238.
Chen, J.S., Ma, E., Harrington, L.B., Da Costa, M., Tian, X., Palefsky, J.M., Doudna, J.A., 2018. Science 360 (6387), 436–439.
Chen, S., Wang, R., Peng, S., Xie, S., Lei, C., Huang, Y., Z, N., 2022. Chem. Sci. 13 (7), 2011–2020.
Chen, Z., Hao, W., Gao, C., Zhou, Y., Zhang, C., Zhang, J., Wang, R., Wang, Y., Wang, S., 2022. Acta Pharm. Sin. B. 12 (8), 3367–3382.
Dai, Y., Wu, Y., Liu, G., Gooding, J.J., 2020. Angew. Chem. Int. Ed. 59 (47), 20754–20766.
Daims, H., Wagner, M., 2007. Appl. Microbiol. Biotechnol. 75 (2), 237–248.
Dong, H., Li, Y., Cheng, J., Xia, Z., Liu, W., Yan, T., Chen, F., Wang, Z., Li, R., Shi, J., S, Q., 2022. Microbiol. Spectr. 10, e0215621.
Earle, K.A., Billings, G., Sigal, M., Lichtman, J.S., Hansson, G.C., Elias, J.E., Amieva, M. R., Huang, K.C., Sonnenburg, J.L., 2015. Cell Host Microbe 18 (4), 478–488.
Elmentaite, R., Kumasaka, N., Roberts, K., Fleming, A., Dann, E., King, H.W., Kleshchevnikov, V., Dabrowska, M., Pritchard, S., Bolt, L., Vieira, S.F., Mamanova, L., Huang, N., Perrone, F., Goh Kai'En, I., Lisgo, S.N., Katan, M., Leonard, S., Oliver, T.R.W., Hook, C.E., Nayak, K., Campos, L.S., Dominguez Conde, C., Stephenson, E., Engelbert, J., Botting, R.A., Polanski, K., van Dongen, S., Patel, M., Morgan, M.D., Marioni, J.C., Bayraktar, O.A., Meyer, K.B., He, X., Barker, R.A., Uhlig, H.H., Mahbubani, K.T., Saeb-Parsy, K., Zilbauer, M., Clatworthy, M.R., Haniffa, M., James, K.R., Teichmann, S.A., 2021. Nature 597 (7875), 250–255.
Feng, W., Newbigging, A.M., Tao, J., Cao, Y., Peng, H., Le, C., Wu, J., Pang, B., Li, J., Tyrrell, D.L., Zhang, H., Le, X.C., 2021. Chem. Sci. 12 (13), 4683–4698.
Gootenberg, J.S., Abudayyeh, O.O., Kellner, M.J., Joung, J., Collins, J.J., Zhang, F., 2018. Science 360 (6387), 439–444.
Gosiewski, T., Ludwig-Galezowska, A.H., Huminska, K., Sroka-Oleksiak, A., Radkowski, P., Salamon, D., Wojciechowicz, J., Kus-Slowinska, M., Bulanda, M., Wolkow, P.P., 2017. Eur. J. Clin. Microbiol. Infect. Dis. 36 (2), 329–336.
Greuter, D., Loy, A., Horn, M., Rattei, T., 2016. Nucleic Acids Res. 44 (D1), D586–D589.
Haldar, J., A, D., Alvarez de Cienfuegos, L., Chen, J., AM, K., 2006. Proc. Natl. Acad. Sci. U. S. A. 103, 17667–17671.
Huang, S., Song, Y., Liang, T., Zhang, J.R., Zhu, J.J., 2021. Small, e2104622.
Kang, Y.K., Kwon, K., Ryu, J.S., Lee, H.N., Park, C., Chung, H.J., 2017. Bioconjugate Chem. 28 (4), 957–967.
Kleinstiver, B.P., Sousa, A.A., Walton, R.T., Tak, Y.E., Hsu, J.Y., Clement, K., Welch, M. M., Horng, J.E., Malagon-Lopez, J., Scarfo, I., Maus, M.V., Pinello, L., Aryee, M.J., Joung, J.K., 2019. Nat. Biotechnol. 37 (3), 276–282.
Knight, S.C., Tjian, R., JA, D., 2017. Angew. Chem. Int. Ed. 57, 4329–4337.
Kwon, S., Sevick-Muraca, E.M., 2017. Contrast Media Mol. Imaging 2017, 7659242.
Kwon, H.Y., Liu, X., Choi, E.G., Lee, J.Y., Choi, S.Y., Kim, J.Y., Wang, L., Park, S.J., Kim, B., Lee, Y.A., Kim, J.J., Kang, N.Y., Chang, Y.T., 2019. Angew. Chem. Int. Ed. 58 (25), 8426–8431.
Laurino, P., Kikkeri, R., Azzouz, N., Seeberger, P.H., 2011. Nano Lett. 11 (1), 73–78.
Lee, M.S., Hyun, H., Park, I., Kim, S., Jang, D.H., Kim, S., Im, J.K., Kim, H., Lee, J.H., Kwon, T., Kang, J.H., 2022. Small Methods 6 (3), e2101239.
Lim, Y., Shiver, A.L., Khariton, M., Lane, K.M., Ng, K.M., Bray, S.R., Qin, J., Huang, K.C., Wang, B., 2019. PLoS Biol. 17 (10), e3000268.
Lin, L., Du, Y., Song, J., Wang, W., Yang, C., 2021a. Acc. Chem. Res. 54 (9), 2076–2087.
Lin, L., Song, J., Li, J., Zuo, X., Wei, H., Yang, C., Wang, W., 2021b. Gut Microb. 13 (1), 1960134.
Liu, W., Miao, L., Li, X., Xu, Z., 2021. Coord. Chem. Rev. 429.
Mark Welch, J.L., Hasegawa, Y., McNulty, N.P., Gordon, J.I., Borisy, G.G., 2017. Proc. Natl. Acad. Sci. U. S. A. 114 (43), E9105–E9114.
Pan, Y., Luan, X., Zeng, F., Xu, Q., Li, Z., Gao, Y., Liu, X., Li, X., Han, X., Shen, J., Song, Y., 2022. Biosens. Bioelectron. 209, 114239.
Parks, D.H., Chuvochina, M., Waite, D.W., Rinke, C., Skarshewski, A., Chaumeil, P.A., Hugenholtz, P., 2018. Nat. Biotechnol. 36 (10), 996–1004.
Pasquina-Lemonche, L., Burns, J., Turner, R.D., Kumar, S., Tank, R., Mullin, N., Wilson, J.S., Chakrabarti, B., Bullough, P.A., Foster, S.J., Hobbs, J.K., 2020. Nature 582 (7811), 294–297.
Peukert, C., Gholap, S.P., Green, O., Pinkert, L., van den Heuvel, J., van Ham, M., Shabat, D., Broenstrup, M., 2022. Angew. Chem. Int. Ed. 61 (25), e202201423.

Pirttilä, A.M., L, H., Pospiech, H., Myllylä, R., Hohtola, A., 2000. Appl. Environ. Microbiol. 66, 3073–3077.
Ranasinghe, R.T., Challand, M.R., Ganzinger, K.A., Lewis, B.W., Softley, C., Schmied, W. H., Horrocks, M.H., Shivji, N., Chin, J.W., Spencer, J., Klenerman, D., 2018. Nat. Commun. 9 (1), 655.
Shang, S., Chen, G., Wu, Y., Du, L., Zhao, Z., 2005. Pediatr. Res. 58 (1), 143–148.
Shi, H., Shi, Q., Grodner, B., Lenz, J.S., Zipfel, W.R., Brito, I.L., De Vlaminck, I., 2020. Nature 588 (7839), 676–681.
Tang, J., Chu, B., Wang, J., Song, B., Su, Y., Wang, H., He, Y., 2019. Nat. Commun. 10 (1), 4057.
Teng, X., Dai, Y., Li, J., 2022. Explorations 2, 20210214.
Valm, A.M., Mark Welch, J.L., Rieken, C.W., Hasegawa, Y., Sogin, M.L., Oldenbourg, R., Dewhirst, F.E., Borisy, G.G., 2011. Proc. Natl. Acad. Sci. U. S. A. 108 (10), 4152–4157.
Wagner, M., Horn, M., Daims, H., 2003. Curr. Opin. Microbiol. 6 (3), 302–309.
Wang, D.-X., Wang, Y.-X., Wang, J., Ma, J.-Y., Liu, B., Tang, A.-N., Kong, D.-M., 2022. Chem. Sci. 13 (15), 4364–4371.
Wu, S., Yu, T., Zhou, R., Liang, Y., Li, Y., Yang, J., Wang, Y., An, J., Qin, S., Zhang, Z., Shi, J., 2021. Nano Today 38, 101185.
Xing, B., Wang, Z., Do, T.C., Zhong, W., Lau, J.W., Kwek, G., Chan-Park, M.B., 2021. Angew. Chem. Int. Ed. 60 (31), 16900–16905.
Zhang, K., Li, Y., Liu, J., Yang, X., Xu, Y., Shi, J., Liu, W., Li, J., 2020. CCS Chem 2 (6), 631–641.
Zhang, L., Chen, J., He, M., Su, X., 2022. Explorations 2, 20210265.